eprints@whiterose.ac.uk
https://eprints.whiterose.ac.uk/

Chemical and Electronic Structure Analysis of a SrTiO$_3$ (001) / *p*-Ge (001) Hydrogen Evolution Photocathode

Kelsey A. Stoerzinger[1,*], Yingge Du[1], Steven R. Spurgeon[2], Le Wang[1], Demie Kepaptsoglou[3,4,5], Quentin M. Ramasse[3,6,7], Ethan J. Crumlin[8], Scott A. Chambers[1,*]

[1] Physical and Computational Sciences Directorate, Pacific Northwest National Laboratory, 902 Battelle Blvd, Richland WA 99352, USA

[2] Energy and Environment Directorate, Pacific Northwest National Laboratory, 902 Battelle Blvd, Richland WA 99352, USA

[3] SuperSTEM, SciTech Daresbury Campus, Daresbury, WA44AD, UK

[4] Jeol Nanocentre, University of York, Heslington, York, YO10 5BR, UK

[5] Department of Physics, University of York, Heslington, York, YO10 5BR, UK

[6] School of Chemical and Process Engineering, University of Leeds, Leeds, LS2 9JT, UK

[7] School of Physics, University of Leeds, Leeds, LS2 9JT, UK

[8] Advanced Light Source, Lawrence Berkeley National Laboratory, Berkeley, California 94720, USA

*kelsey.stoerzinger@pnnl.gov; sa.chambers@pnnl.gov

Abstract

Germanium is a small-gap semiconductor that efficiently absorbs visible light, resulting in photoexcited electrons predicted to be sufficiently energetic to reduce H$_2$O and evolve H$_2$ gas. In order to protect the surface from corrosion and prevent surface charge recombination in contact with aqueous pH 7 electrolyte, we grew epitaxial SrTiO$_3$ layers of different thicknesses

1

on *p*-Ge (001) surfaces. 4 nm $SrTiO_3$ allows photogenerated electrons to reach the surface and evolve H_2 gas, while 13 nm $SrTiO_3$ blocks these electrons. Ambient pressure X-ray photoelectron spectroscopy indicates the surface readily dissociates H_2O to form OH species, which may impact surface band bending.

Keywords electrochemical synthesis; surface chemistry; Ge

Introduction

The direct conversion of solar energy to chemical fuels is a tantalizing route to store renewable energy. By employing photocatalysts to split water into H_2 and O_2 gas,[1-2] this can be achieved in a cycle free of CO_2 emissions. A 'Z-scheme'[3-4] separates the two constituent reactions—the oxygen evolution reaction (OER) and hydrogen evolution reaction (HER)—so that they occur on separate electrodes, thus decoupling the requirements of band gap and the energy of photoexcited carriers in materials design. Typical oxide photoanodes used to drive the OER have large band gaps,[5-7] and can thus absorb high-energy photons in a photoelectrochemical (PEC) device, allowing low-energy photons to pass through to the photocathode, which drives the HER.

One semiconductor with attractive light-absorption properties is Ge. In contrast to other semiconductors currently being studied, Ge has a small, indirect band gap of 0.66 eV, as well as a larger optical absorption coefficient across the visible portion of the solar spectrum and into the infrared.[8] Furthermore, Ge exhibits high room-temperature electron and hole mobilities of 3900 and 1900 cm^2/V.s, respectively.[9] Density functional theory (DFT) calculations indicate that the

2

conduction band of Ge is higher in energy than hydrogen redox,[10] indicating photoexcited electrons are energetic enough to reduce H_2O to evolve H_2 gas. However, interaction with the electrolyte can lead to corrosion of the Ge surface[11] and recombination of photogenerated electron-hole pairs at surface states,[12] limiting PEC activity.

We employ controlled passivation[13] of Ge by epitaxial growth of a wide band-gap semiconductor, $SrTiO_3$, using oxide molecular beam epitaxy (MBE). By examining a model epitaxial film, we are able to examine charge transport through the heterostructure to yield a critical new understanding of PEC. A similar approach has recently been employed to protect a GaAs photovoltaic.[14] Growth of $SrTiO_3$ on Ge has previously been demonstrated for the purpose of investigating associated electrical properties,[15-16] and we have recently measured the valence band (VB) offset between Ge and $SrTiO_3$.[17] These findings support the idea that photoexcited electrons in the Ge would have a downhill path in energy to reach the $SrTiO_3$ surface.

Here we present the first PEC measurements of the HER on a $SrTiO_3$ (001) / p-Ge (001) heterostructure in neutral (pH 7) electrolyte. This model epitaxial system enables quantification of the abrupt interface by scanning transmission electron microscopy (STEM), as well as surface stoichiometry and speciation, both post mortem, following electrochemical cycling, and *in situ* using ambient pressure X-ray photoelectron spectroscopy[18] (AP-XPS). The Sr/Ti ratio remains similar under all conditions, suggesting the $SrTiO_3$ film is stable in the electrochemical environment and supporting its role as a protective cap on Ge, and the surface actively dissociates H_2O to form OH groups. Surface roughness on the Ge substrate leads to pinhole defects which hinder the efficacy of 4-nm $SrTiO_3$ film passivation; however, a 13 nm $SrTiO_3$ film blocks electron transport to the surface. These findings suggest that tailoring $SrTiO_3$

3

electronic properties by, for example, doping, may provide a promising route for Ge photocathode protection.

Experimental Details

Film Growth

Ga-doped *p*-Ge (001) substrates (AXT Inc., $\rho = 0.04$ Ω-cm) were prepared by wet etching procedures described elsewhere.[19] Following desorption of the chemically prepared oxide at ~600 °C, the surfaces were clean at the detection limit of X-ray photoelectron spectroscopy (XPS) and exhibited a (2×1) reconstructed surface. Epitaxial growth by oxygen assisted MBE followed the approach outlined in Jahangir-Moghadam et al.[20], as further detailed in Ref. [17]. An initial SrGe$_2$ (001) (3×1) layer was grown at 400 °C in vacuum, followed by the growth of 3 unit cells (u.c.) amorphous SrTiO$_3$ at ambient temperature in 4×10^{-7} Torr O$_2$, followed by subsequent crystallization at 600 °C in vacuum. Additional layers were grown at 300 °C in O$_2$ and annealed at up to 500 °C in vacuum to achieve better crystallinity, reaching a final thickness of 5 u.c. (2 nm), 4 nm, or 13 nm SrTiO$_3$.

Scanning Transmission Electron Microscopy

Cross-sectional scanning transmission electron microscopy (STEM) samples were prepared using an FEI Helios NanoLab Dual-Beam Focused Ion Beam (FIB) microscope and a standard lift out procedure along the Ge [100] and [110] zone axes, with initial cuts made at 30 kV / 2° and final polishing at 1 kV / 3° incidence angles. High-angle annular dark field (STEM-HAADF) images were collected on a JEOL ARM-200CF microscope operating at 200 kV, with a convergence semiangle of 20.6 mrad and a collection inner semiangle ranging from 68–90 mrad. To minimize scan artifacts and improve signal-to-noise, drift-corrected images were

4

prepared using the SmartAlign plugin;[21] for this, a series of 10 frames at 1024 x 1024 pixels with a fast 2 μs px^{-1} dwell time and 90º rotation between frames was used. The frames were upsampled 3x prior to non-rigid alignment. The inset of Figure 1c was subsequently processed using a lattice enhanced filter to improve signal-to-noise.[22]

Electron energy loss spectroscopy (STEM-EELS) maps were collected on a Nion UltraSTEM 100MC "Hermes" microscope operating at 60 kV with a convergence semiangle of 31 mrad and a 44 mrad STEM-EELS collection angle. STEM-EELS maps were collected using 0.37 eV ch^{-1} dispersion, yielding an effective energy resolution of ~1.1 eV. No plural scattering correction was performed, since zero loss measurements confirm that the samples are sufficiently thin (t /λ < 0.5 inelastic mean free paths). Composition maps are presented in the supplementary information.

Photoelectrochemistry

Films were transferred directly from UHV to a N_2-purged glove box for PEC measurements. GaIn eutectic (Sigma, >99.99%) was scratched into the back of the Ge, and a Cu wire held in contact with the pad in a custom-built compression cell. The electrolyte was prepared from Nanopure water (18.2 MΩ-cm) from a mixture of K_2HPO_4 and KH_2PO_4 (Sigma, >99.0%) to achieve a pH of 7 and phosphate concentration of 0.1 M, and bubbled with ultra-high purity N_2 gas before and during data collection. Measurements were made with a CHI-660C potentiostat by cyclic voltammetry at 20 mV/s or constant potential measurements, and voltages corrected for the electrolyte resistance between the working and reference electrodes (~95 Ω for 4 nm $SrTiO_3$/Ge). The saturated calomel reference electrode (RE-2BP, ALS Co.) was calibrated to the reversible hydrogen electrode (RHE) scale in the same electrolyte, saturated with H_2 and

5

using Pt working and counter electrodes. A Pt counter electrode (ALS Co.) was also used for PEC measurements.

Light from a 630 nm ultra-high power LED (Prizmatix) was incident through a planar quartz window. The illuminated area of the sample was defined by the PEEK holder, and was commensurate with the area exposed to the electrolyte. The intensity of the LED at the location of the sample was measured after passing through the quartz window with a Newport 843-R power meter, and estimated to attenuate ~10% over the ~6 cm path length from water absorption.

X-ray Photoelectron Spectroscopy

Characterization of the films as-grown and after (photo)electrochemical cycling was performed with an Al K-alpha source in UHV at room-temperature.

Ambient pressure X-ray photoelectron Spectroscopy (AP-XPS) was collected at Beamline 9.3.2 at Lawrence Berkeley National Laboratory's (LBNL) Advanced Light Source (ALS).[23] 5 u.c. $SrTiO_3$ / Ge was placed directly onto a ceramic heater, held in place by spring-loaded Inconel tips separated with an Al_2O_3 spacer, and grounded through the thermocouple. The thermocouple was pressed into a gold foil placed directly onto the sample surface and isolated from the sample holder clip with an Al_2O_3 spacer.
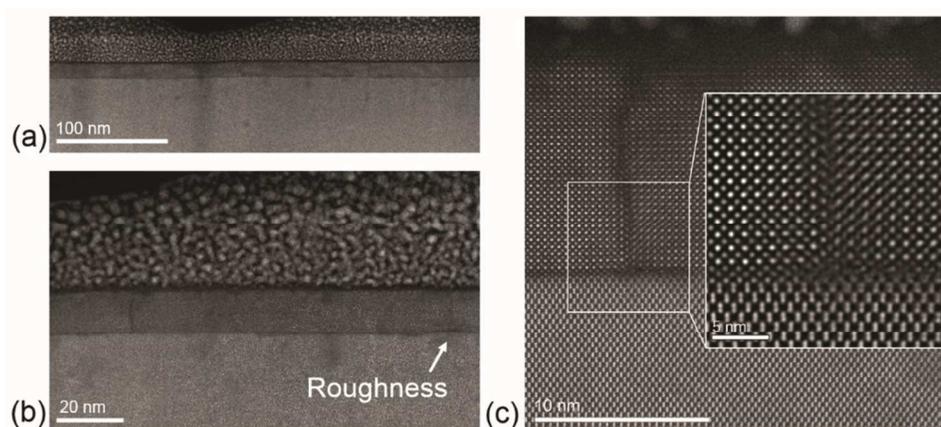
The incident photon energy was calibrated to the Au $4f_{5/2}$ peak at 84 eV binding energy (BE). The sample was first heated to 300 °C in 100 mTorr O_2 (measured by a calibrated membrane pressure gauge) and characterized. Keeping the sample at 300 °C, the chamber was evacuated to a pressure lower than 1.5×10^{-7} Torr, and 100 mTorr H_2O was introduced into the chamber. The water source was prepared from deionized water (Millipore, >18.2 MΩ·cm) and degassed by several freeze–pump–thaw cycles. The sample was then cooled in 100 mTorr H_2O.

6

O 1s spectra were deconvoluted with Gaussian–Lorentzian (GL) peaks using CasaXPS after a Shirley-type background subtraction (**Table S1**). The O 1s integrated area of the (bi)carbonate peak was calculated from the area of the C 1s (bi)carbonate peak using an O 1s:C 1s relative sensitivity factor, which was experimentally calibrated using the core levels of CO_2 gas.[24]
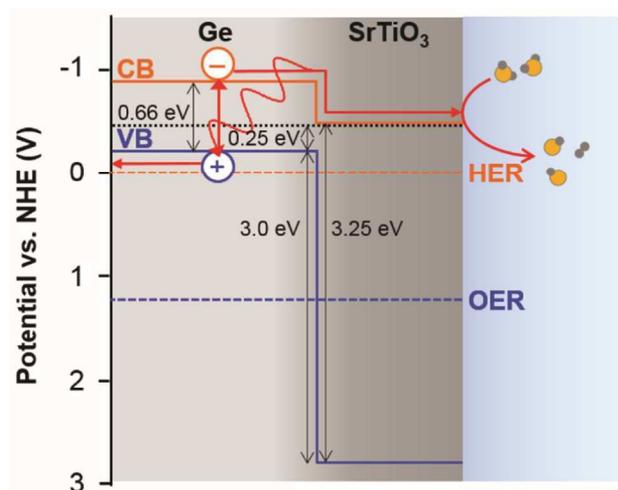
Results

Figure 1 shows representative cross-sectional STEM-HAADF images that illustrate the quality of the $SrTiO_3$ (001) / p-Ge (001) film and interface. We observe a relatively uniform film across large areas, as shown in the image of a 13 nm $SrTiO_3$ / Ge interface in Figure 1a. We observe no phase separation or impurities, but we do measure some substrate roughness in Figure 1b. This roughness is accompanied by film discontinuities and the presence of antiphase boundaries (see inset of Figure 1c). We note that the damage at the film surface (top) in this image is the result of long exposure to the electron beam and not characteristic of the film itself.

We found that this structure is highly beam sensitive at 200 kV and that exposure to the electron beam over 30–60 seconds was sufficient to locally amorphize the structure. To mitigate this problem, we conducted multi-frame, drift-corrected imaging using the SmartAlign plugin[21, 25] to reduce the effective electron dose rate; this approach allowed us to acquire high-resolution images of the film-substrate interface without damaging the underlying structure. Figure 1c shows that the interface is extremely abrupt, a finding further supported by STEM-EELS maps of a related 5 u.c. $SrTiO_3$ / Ge heterostructure shown in Figure S1; these measurements were performed at a lower 60 kV accelerating voltage to avoid excessive sample damage. Taken together, our results illustrate the uniformity, relatively good quality, and sharp interface structure that can be attained through MBE growth of these films.

7

FIG. 1. (a) Representative cross-sectional STEM-HAADF image of a 13 nm $SrTiO_3$ / p-Ge (001) heterostructure, showing the overall structure along the Ge [110] zone-axis. (b) STEM-HAADF image of local Ge substrate roughness. (c) Drift-corrected STEM-HAADF image of a film discontinuity and lattice-filtered inset of an antiphase boundary between two film regions.
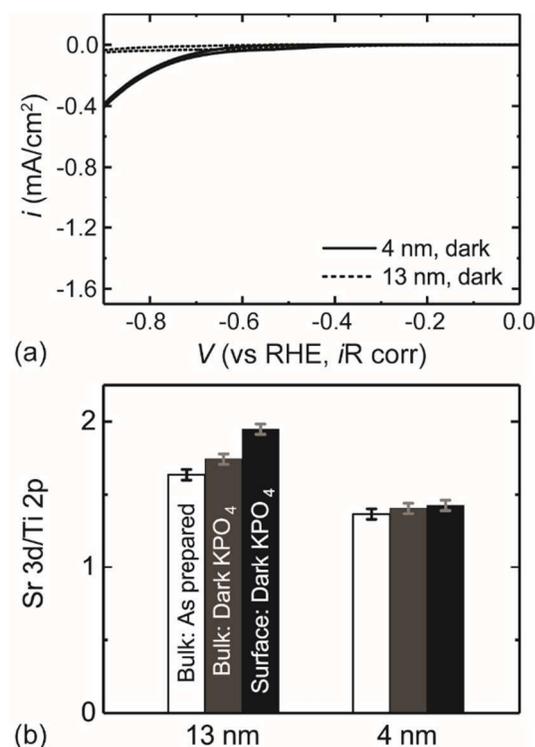
The band alignment at the $SrTiO_3$ / Ge interface is of critical importance for separation of photogenerated electrons and holes, and the transport of electrons to the surface to reduce H_2O and generate H_2. Previous measurement of the core levels and valence band (VB) by XPS[17] indicate the VB of $SrTiO_3$ is 3.0 eV lower in energy than that of p-Ge. Coupled with the 3.25 eV band gap of $SrTiO_3$ and the 0.66 eV band gap of Ge, the conduction band (CB) of $SrTiO_3$ is found to be 0.4 eV below that of Ge. DFT band edge calculations report the Ge CB to be -0.9 V vs. NHE at pH 0,[10] placing the CB of $SrTiO_3$ in the heterostructure at -0.5 vs. NHE (Figure 2). This is in contrast to the CB of isolated $SrTiO_3$, reported at -0.26 V vs. NHE at pH 0.[4] Assuming a Nernstian shift of the oxide band edges with pH,[26] this finding then suggests the CB of the $SrTiO_3$ / Ge heterostructures is at -0.5 V vs. RHE in pH 7, resulting in photoexcited electrons being sufficiently energetic to drive the HER.

FIG. 2. Interface band energy alignment on the NHE scale (pH = 0), obtained from the experimental measurement of VB offset in the heterostructure,[17] reported CB level of Ge[10] and band gap of $SrTiO_3$. For pH 7 conditions, assuming Nernstian behavior of the oxide band edges would then result in a $SrTiO_3$ CB at -0.5 V vs. RHE.
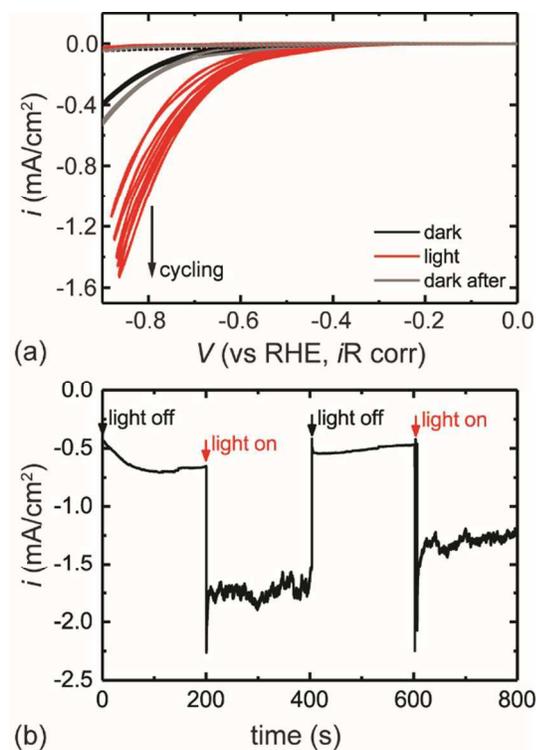
Following growth, the heterojunctions were transferred directly from UHV to a N_2-purged glove box for electrochemical characterization in a custom 3-electrode cell. The pH 7 phosphate-buffered electrolyte was constantly bubbled with N_2 before and during measurements to minimize buildup of evolved H_2 gas. Figure 3 a compares the cyclic voltammetry for 4 nm and 13 nm $SrTiO_3$ on Ge, measured initially in the dark. For the 4 nm film, cathodic current was observed commensurate with the formation of bubbles on the electrode with an onset potential ~ -0.7 V vs. RHE in the dark. For the 13 nm film, current was negligible within the tested window. We hypothesize the 13 nm film acts as a blocking electrode for photogenerated electrons as seen by the larger resistance measured by high frequency impedance spectroscopy at open circuit conditions (> 400 Ω, compared to < 100 Ω for the 4 nm heterostructure).

9

Films were then removed from the electrolyte within the purged N_2 box, rinsed with DI water, dried, and returned to UHV for XPS characterization. XPS confirms no electrodeposition of Pt or other contaminants on the film (Figure S2-S3). The ratio of Sr 3d to Ti 2p core levels remained similar to that of the as-prepared film (Figure 3b), indicating no preferential leaching of e.g. Sr occurred. This is in contrast to thermodynamic calculations of the Pourbaix diagram at pH 7 which indicate a greater stability of TiO_2 with Sr cations compared to $SrTiO_3$,[27] and suggests additional contributors to kinetic stabilization like surface energy and functionalization play an important role. We note, however that the ratio of the Sr 3d and Ti 2p relative to the Ge 3d for the 4 nm film (where the Ge 3d is observable due to the large probe depth of the > 1400 eV kinetic energy photoelectrons) decreased after cycling (Figure S4), suggesting the roughness of the Ge substrate may expose some pinholes defects in the $SrTiO_3$ film which grow with cycling.

FIG. 3. (a) CV curves in dark at 20 mV/s in pH 7, 0.1 M phosphate buffer. The 13 nm SrTiO$_3$ (dashed) acts as a blocking electrode, while the 4 nm film (solid) allows current to be passed to drive HER at high overpotentials. (b) XPS ratio of Sr 3d/Ti 2p core levels measured with $hv = $ 1486 eV for the as prepared heterostructure (white) and after cycling in the dark. At 90° incidence ("bulk") the probe depth is ~7 nm, while at 20° incidence ("surface") it is ~2 nm.

Upon illumination with an ~ 8 mW 630 nm LED (Figure 4a), the 13 nm SrTiO$_3$/Ge heterostructure exhibited no change in current density compared to cycling in the dark. In contrast, the 4 nm SrTiO$_3$/Ge heterostructure exhibited a cathodic photocurrent after initially sweeping below ~ -0.75 V vs. RHE. The photocurrent increased with cycle number; however, the dark current remained constant before and after cycling. We hypothesize this behavior might result from *in situ* generation of oxygen vacancies in the SrTiO$_3$ film, which would facilitate electron transport to the surface. Chronoamperometry (Figure 4b) illustrates the photocurrent from the 4 nm SrTiO$_3$/Ge heterostructure directly by switching the LED on and off, in contrast to the lack of HER photocurrent from a bare Ge wafer (Figure S5). The difference between the dark current just before 200 s and the current during illumination after 200 s (where the noise arises from the rapid generation of H$_2$ bubbles and light scattering) gives a photocurrent of 1.1 mA/cm^2 at -0.87 V vs. RHE. This corresponds to an incident-photon-to-current efficiency (IPCE) of ~14 %. We note that the epitaxial nature of the film on the single crystal Ge substrate results in a roughness factor approaching unity and a highly reflective surface; thus the photocurrent on a geometric basis and IPCE would be expected to improve greatly by introducing nanostructuring.[28] Furthermore, the high overpotential is expected to decrease substantially upon incorporation of a cocatalyst.[29-31]

11

FIG. 4. (a) CVs at 20 mV/s in pH 7, 0.1 M phosphate buffer for the 13 nm SrTiO$_3$ (dashed) and 4 nm SrTiO$_3$ (solid) on Ge. Compared to polarization in the dark (black), illumination with a 630 nm LED (red) causes a photocurrent/voltage for the 4 nm film, which increases with cycling. After illumination (gray), the CV is similar to before illumination. (b) Chronoamperometry for 4 nm SrTiO$_3$ / Ge at -0.87 V vs RHE. The dark HER current initially increases, and illumination leads to a constant -1.75 mA/cm^2 current. Turning the light off returns the current to that previously measured in dark. Repeated illumination gives a similar photocurrent, however this decreases over time.
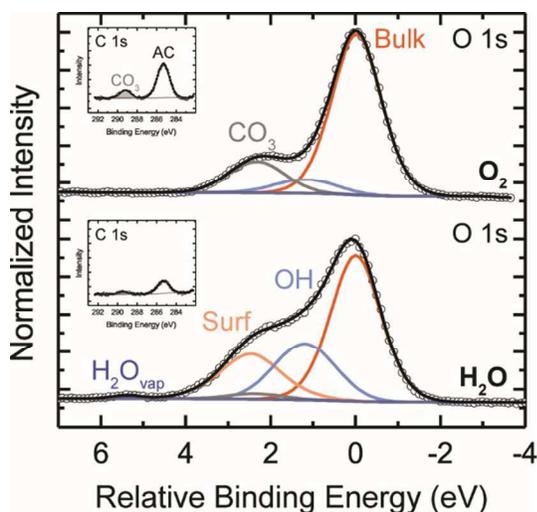
The activity of the 4 nm SrTiO$_3$ / Ge heterostructure decreased with time. Following removal from the cell and copious rinsing to remove salt before introduction to the UHV chamber for XPS, much of the film delaminated, suggesting that pinhole defects in the 4 nm film arising from roughness of the Ge crystal grow with cycling. In contrast, the 13 nm SrTiO$_3$ film

12

shows comparable ratios of Sr 3d and Ti 2p and remains sufficiently thick that no Ge 3d is observed following cycling under illumination (Figure S6). Future directions will include cation-doping of thicker $SrTiO_3$ films to ensure *n*-type conductivity persists over the conformal film thickness.

In order to better understand the interface between $SrTiO_3$ and the electrolyte, we performed ambient pressure X-ray photoelectron spectroscopy (AP-XPS) in both dry-oxidizing and humid-reducing environments. The tunable incident photon energy (IPE) at a synchrotron allows the probe depth to be tuned to the top ~1 nm of the film (hv = 690 eV, O 1s core level), and a system of differential pumping and electrostatic lensing enables the surface speciation to be probed in equilibrium with a gas.[18]

We first consider the surface at 300 °C in 100 mTorr of O_2, similar to growth conditions, which minimizes carbon present from transferring the samples between growth facilities and the synchrotron (Figure S7). Figure 5 illustrates that the O 1s spectra is dominated by bulk-coordinated oxygen of the perovskite crystal,[24] with some residual CO_3 whose intensity is scaled from that of the CO_3 feature in the C 1s inset. When the O_2 is removed from the chamber and H_2O slowly introduced, a feature increases in intensity at ~1.2 eV BE above the bulk (Figure S8). This feature is attributed to hydroxyl, OH, formation from the dissociation of H_2O on the surface.[24] In a humid environment, a feature ("Surf") at higher BE above the bulk is notable, observed from depth profiling (Figure S9) to be located at the surface. A feature at similar BE offsets located on the surface has been observed for (001)-oriented $LaFeO_3$ films terminated with the "LaO" plane, but not for the "FeO_2" plane,[32] We note, however, that on the $SrTiO_3$ surface, a small phosphorous signal (likely in the form of phosphate) was observed in humid environments (Figure S7), and may also contribute to the signal at this intensity. Adsorption of

13

phosphate species in humid environments may also have implications on the use and role of a

PO_4-containing buffer during PEC measurements.[33]

FIG. 5. AP-XPS performed at an incident photon energy (IPE) of $h\nu = 690$ eV at 300 °C in 100

mTorr O_2 (top) or 100 mTorr H_2O (bottom). The O 1s spectra is shown on a binding energy (BE)

scale relative to bulk oxygen (orange), with OH (light blue), CO_3 (gray, intensity determined

from the shaded CO_3 feature in the C 1s inset), surface oxygen (peach), and H_2O_{vapor} (medium

blue) at increasingly higher BE. Some adventitious carbon (AC, C 1s inset) remains and

attenuates the spectra. Fitting parameters are given in Table S1.

The notable dissociation of H_2O on the surface of $SrTiO_3$ to form OH species suggests

that during PEC conditions in a neutral electrolyte, $SrTiO_3$ is likely also hydroxylated. This

adsorption of OH species may in turn impact band bending at the surface, of future interest for

studies linking surface speciation to the driving force for charge transfer during PEC. In further

consideration of the surface stoichiometry in equilibrium with gaseous environments, the ratio of

Sr signal to combined Sr and Ti signals remains relatively constant across both dry-oxidizing and

humid-reducing conditions, as does the distribution of Sr and Ti with depth (Figure S10). This

further supports *ex situ* measurements after electrochemically cycling, which indicate Sr remains stable within the $SrTiO_3$ film in contact with H_2O at pH 7.

Conclusions

$SrTiO_3$ was epitaxially grown on *p*-Ge (001) using MBE as a means to protect the surface of the Ge photoabsorber during PEC measurements in aqueous pH 7 electrolyte and maintain an energetically downhill path for photogenerated electrons to reach the solution. The band alignment between $SrTiO_3$ and Ge is such that photoexcited electrons can travel through a 4 nm $SrTiO_3$ capping layer and remain sufficiently energetic to reduce H_2O and evolve H_2 gas in the HER reaction. For 13 nm $SrTiO_3$, the film behaves like a blocking electrode, with larger contact resistance and minimal current passed at similar overpotentials compared to the 4 nm film. At -0.87 V vs RHE, the IPCE for 630 nm red light is ~14%, noting that the roughness factor of the epitaxial film approaches one and notable reflective losses are not considered in calculation of the IPCE. Thus, the current density would be expected to improve with nanostructuring. Furthermore, the electrode is free of Pt or any other catalyst, and thus its probed intrinsic ability to supply photoexcited electrons to the HER is expected to notably improve upon deposition of a co-catalyst. Some inherent roughness (on the nm scale) on the Ge surface leads to the presence of pinhole defects in the 4 nm film, resulting in corrosion and film delamination. Future directions include La doping of the $SrTiO_3$ films to control their carrier concentration such that thicker conformal films can be epitaxially grown and maintain sufficient conductivity for charge transfer.

In situ characterization of the $SrTiO_3$ (001) / *p*-Ge (001) heterostructure provides insight into the surface speciation during reaction conditions. AP-XPS was used to characterize the surface under dry-oxidizing and humid-reducing conditions. In contrast to the dry O_2

15

environment, in a humid environment $SrTiO_3$ notably dissociates H_2O to form OH species. This indicates that during the HER in pH 7 aqueous electrolyte, the $SrTiO_3$ surface likely also contains some hydroxyl species. Future directions will link this speciation to the resultant surface band bending.

Acknowledgements

References

1.   T.R. Cook, D.K. Dogutan, S.Y. Reece, Y. Surendranath, T.S. Teets and D.G. Nocera: Solar energy supply and storage for the legacy and nonlegacy worlds. *Chem. Rev.* **110**, 6474-6502 (2010).

2.   M.G. Walter, E.L. Warren, J.R. McKone, S.W. Boettcher, Q. Mi, E.A. Santori and N.S. Lewis: Solar water splitting cells. *Chem. Rev.* **110**, 6446-6473 (2010).

3.   A. Kudo and Y. Miseki: Heterogeneous photocatalyst materials for water splitting. *Chem. Soc. Rev.* **38**, 253-278 (2009).

4.   J. Li and N. Wu: Semiconductor-based photocatalysts and photoelectrochemical cells for solar fuel generation: A review. *Catal. Sci. Technol.* **5**, 1360-1384 (2015).

5.   B.D. Alexander, P.J. Kulesza, I. Rutkowska, R. Solarska and J. Augustynski: Metal oxide photoanodes for solar hydrogen production. *J. Mater. Chem.* **18**, 2298-2303 (2008).

6.   K. Sivula and R. van de Krol: Semiconducting materials for photoelectrochemical energy conversion. *Nat. Rev. Mater.* **1**, 15010 (2016).

7.   W.A. Smith, I.D. Sharp, N.C. Strandwitz and J. Bisquert: Interfacial band-edge energetics for solar fuels production. *Energy Environ. Sci.* **8**, 2851-2862 (2015).

8.   S.M. Sze, *Physics of semiconductor devices*. John Wiley and Sons: 1981.

9.   M.B. Prince: Drift mobilities in semiconductors. I. Germanium. *Phys. Rev.* **92**, 681-687 (1953).

10.   S. Chen and L.-W. Wang: Thermodynamic oxidation and reduction potentials of photocatalytic semiconductors in aqueous solution. *Chem. Mater.* **24**, 3659-3666 (2012).

11.   V.R. Erdélyi and M. Green: Hydrogen overpotential on germanium electrodes. *Nature* **182**, 1592 (1958).

17

12.   R. Memming and G. Neumann: Electrochemical reduction and hydrogen evolution on germanium electrodes. *J. Electroanal. Chem. Interfacial Electrochem.* **21**, 295-305 (1969).

13.   S. Hu, N.S. Lewis, J.W. Ager, J. Yang, J.R. McKone and N.C. Strandwitz: Thin-film materials for the protection of semiconducting photoelectrodes in solar-fuel generators. *J. Phys. Chem. C* **119**, 24201-24228 (2015).

14.   L. Kornblum, D.P. Fenning, J. Faucher, J. Hwang, A. Boni, M.G. Han, M.D. Morales-Acosta, Y. Zhu, E.I. Altman, M.L. Lee, C.H. Ahn, F.J. Walker and Y. Shao-Horn: Solar hydrogen production using epitaxial $SrTiO_3$ on a GaAs photovoltaic. *Energy Environ. Sci.* **10**, 377-382 (2017).

15.   M.K. Hudait, M. Clavel, Y. Zhu, P.S. Goley, S. Kundu, D. Maurya and S. Priya: Integration of $SrTiO_3$ on crystallographically oriented epitaxial germanium for low-power device applications. *ACS Appl. Mater. Interfaces* **7**, 5471-5479 (2015).

16.   M.D. McDaniel, T.Q. Ngo, A. Posadas, C. Hu, S. Lu, D.J. Smith, E.T. Yu, A.A. Demkov and J.G. Ekerdt: A chemical route to monolithic integration of crystalline oxides on semiconductors. *Adv. Mater. Interfaces* **1**, 1400081-n/a (2014).

17.   S.A. Chambers, Y. Du, R.B. Comes, S.R. Spurgeon and P.V. Sushko: The effects of core-level broadening in determining band alignment at the epitaxial $SrTiO_3(001)$/p-Ge(001) heterojunction. *App. Phys. Lett.* **110**, 082104 (2017).

18.   K.A. Stoerzinger, W.T. Hong, E.J. Crumlin, H. Bluhm and Y. Shao-Horn: Insights into electrochemical reactions from ambient pressure photoelectron spectroscopy. *Acc. Chem. Res.* **48**, 2976-2983 (2015).

19.   P. Ponath, A.B. Posadas, R.C. Hatch and A.A. Demkov: Preparation of a clean Ge(001) surface using oxygen plasma cleaning. *J. Vac. Sci. Technol., B: Nanotechnol. Microelectron.: Mater., Process., Meas., Phenom.* **31**, 031201 (2013).

20.   M. Jahangir-Moghadam, K. Ahmadi-Majlan, X. Shen, T. Droubay, M. Bowden, M. Chrysler, D. Su, S.A. Chambers and J.H. Ngai: Band-gap engineering at a semiconductor–crystalline oxide interface. *Adv. Mater. Interfaces* **2**, 1400497-n/a (2015).

21.   L. Jones, H. Yang, T.J. Pennycook, M.S.J. Marshall, S. Van Aert, N.D. Browning, M.R. Castell and P.D. Nellist: Smart align—a new tool for robust non-rigid registration of scanning microscope data. *Advanced Structural and Chemical Imaging* **1**, 8 (2015).

22.   O.L. Krivanek, M.F. Chisholm, V. Nicolosi, T.J. Pennycook, G.J. Corbin, N. Dellby, M.F. Murfitt, C.S. Own, Z.S. Szilagyi, M.P. Oxley, S.T. Pantelides and S.J. Pennycook: Atom-by-atom structural and chemical analysis by annular dark-field electron microscopy. *Nature* **464**, 571 (2010).

23.   M.E. Grass, P.G. Karlsson, F. Aksoy, M. Lundqvist, B. Wannberg, B.S. Mun, Z. Hussain and Z. Liu: New ambient pressure photoemission endstation at advanced light source beamline 9.3.2. *Rev. Sci. Instrum.* **81**, 053106 (2010).

24.   K.A. Stoerzinger, W.T. Hong, E.J. Crumlin, H. Bluhm, M.D. Biegalski and Y. Shao-Horn: Water reactivity on the $LaCoO_3$ (001) surface: An ambient pressure x-ray photoelectron spectroscopy study. *J. Phys. Chem. C* **118**, 19733-19741 (2014).

25.   L. Jones, A. Varambhia, R. Beanland, D. Kepaptsoglou, I. Griffiths, A. Ishizuka, F. Azough, R. Freer, K. Ishizuka, D. Cherns, Q.M. Ramasse, S. Lozano-Perez and P.D. Nellist: Managing dose-, damage- and data-rates in multi-frame spectrum-imaging. *Microscopy (In press)*, DOI 10.1093/jmicro/dfx125 (2018).

19

26.   Y. Ping, R. Sundararaman and W.A. Goddard III: Solvation effects on the band edge positions of photocatalysts from first principles. *Phys. Chem. Chem. Phys.* **17**, 30499-30509 (2015).

27.   I.E. Castelli, K.S. Thygesen and K.W. Jacobsen: Calculated pourbaix diagrams of cubic perovskites for water splitting: Stability against corrosion. *Top. Catal.* **57**, 265-272 (2014).

28.   L.N. Quan, Y.H. Jang, K.A. Stoerzinger, K.J. May, Y.J. Jang, S.T. Kochuveedu, Y. Shao-Horn and D.H. Kim: Soft-template-carbonization route to highly textured mesoporous carbon-tio$_2$ inverse opals for efficient photocatalytic and photoelectrochemical applications. *Phys. Chem. Chem. Phys.* **16**, 9023-9030 (2014).

29.   K.C. Kwon, S. Choi, K. Hong, D.M. Andoshe, J.M. Suh, C. Kim, K.S. Choi, J.H. Oh, S.Y. Kim and H.W. Jang: Tungsten disulfide thin film/p-type Si heterojunction photocathode for efficient photochemical hydrogen production. *MRS Commun.* **7**, 272-279 (2017).

30.   J.E. Thorne, Y. Zhao, D. He, S. Fan, S. Vanka, Z. Mi and D. Wang: Understanding the role of co-catalysts on silicon photocathodes using intensity modulated photocurrent spectroscopy. *Phys. Chem. Chem. Phys.* **19**, 29653-29659 (2017).

31.   D.V. Esposito, I. Levin, T.P. Moffat and A.A. Talin: H$_2$ evolution at Si-based metal–insulator–semiconductor photoelectrodes enhanced by inversion channel charge collection and H spillover. *Nat. Mater.* **12**, 562 (2013).

32.   K.A. Stoerzinger, R. Comes, S.R. Spurgeon, S. Thevuthasan, K. Ihm, E.J. Crumlin and S.A. Chambers: Influence of LaFeO$_3$ surface termination on water reactivity. *J. Phys. Chem. Lett.* **8**, 1038-1043 (2017).

33.   M. Favaro, F.F. Abdi, M. Lamers, E.J. Crumlin, Z. Liu, R. van de Krol and D.E. Starr: Light-induced surface reactions at the bismuth vanadate/potassium phosphate interface. *J. Phys. Chem. B*, **122**, 801–809 (2018).

21

Supplemental Information for:

Chemical and Electronic Structure Analysis of a SrTiO₃ (001) / p-Ge (001) Hydrogen Evolution Photocathode

Kelsey A. Stoerzinger[1,*], Yingge Du[1], Steven R. Spurgeon[2], Le Wang[1], Demie Kepaptsoglou[3,4,5], Quentin M. Ramasse[3,6,7], Ethan J. Crumlin[8], Scott A. Chambers[1,*]

[1] Physical and Computational Sciences Directorate, Pacific Northwest National Laboratory, 902 Battelle Blvd, Richland WA 99352, USA

[2] Energy and Environment Directorate, Pacific Northwest National Laboratory, 902 Battelle Blvd, Richland WA 99352, USA

[3] SuperSTEM, SciTech Daresbury Campus, Daresbury, WA44AD, UK

[4] Jeol Nanocentre, University of York, Heslington, York, YO10 5BR, UK
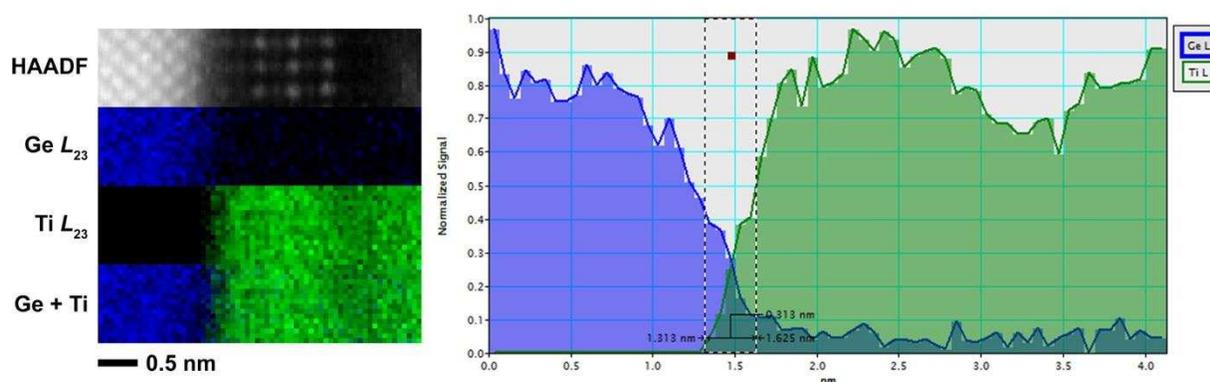
[5] Department of Physics, University of York, Heslington, York, YO10 5BR, UK

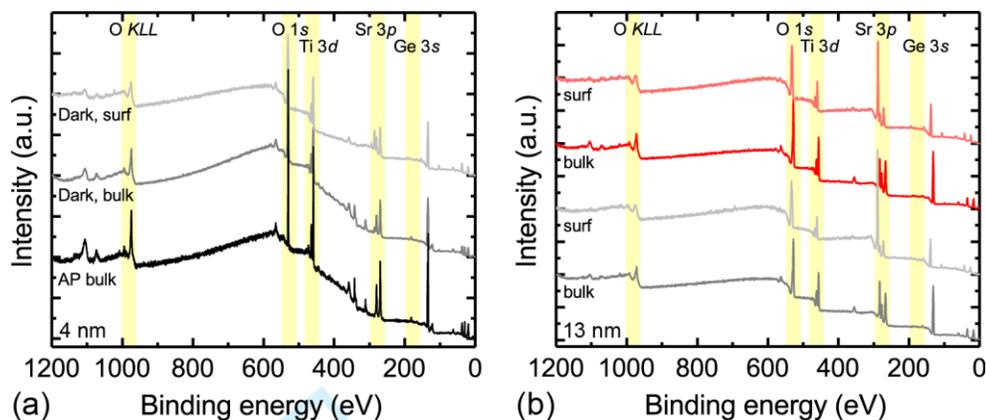[6] School of Chemical and Process Engineering, University of Leeds, Leeds, LS2 9JT, UK

[7] School of Physics, University of Leeds, Leeds, LS2 9JT, UK

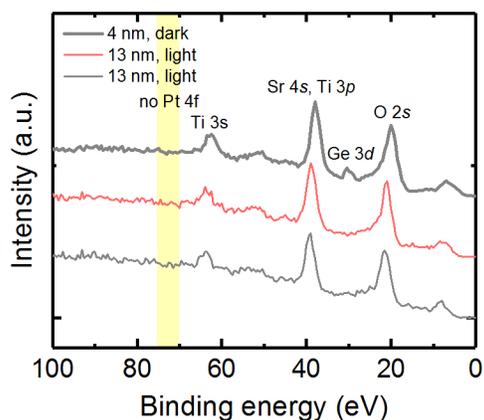[8] Advanced Light Source, Lawrence Berkeley National Laboratory, Berkeley, California 94720, USA
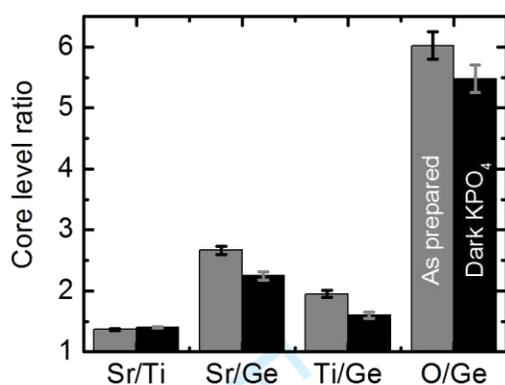
*kelsey.stoerzinger@pnnl.gov; sa.chambers@pnnl.gov

Figure S1: Left: STEM-EELS composition maps of a 5 u.c. SrTiO₃ / p-Ge (001) film measured at 60 kV, showing the integrated Ge L₂,₃ and Ti L₂,₃ edge signals along the Ge [100] zone-axis. Right: Line profiles extracted from the maps, highlighting the sharp interface between the film and substrate. The maps have been normalized to the signal extrema on either side of the interface. Some beam damage has occurred near the surface (right side) of the map.
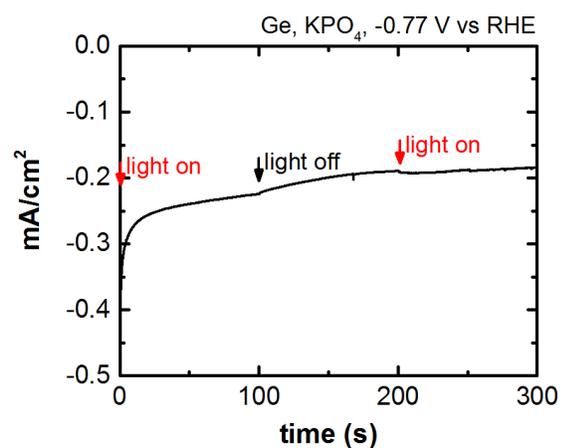
S1

Figure S2: Surveys with an Al K-alpha source (IPE hv = 1486 eV) at 90° (bulk) and 20° (surf) incidence. highlighting some of the key core level and Auger features. (a) For 4 nm $SrTiO_3$ / Ge, a small amount of Ge intensity (core levels and Auger features) can be observed through the thickness of the 4 nm film due to the large information depth of high kinetic energy photoelectrons. (b) For 13 nm $SrTiO_3$ / Ge, no Ge is observed. On both films, carbon is present after measurements in both the dark (gray) and light (red).
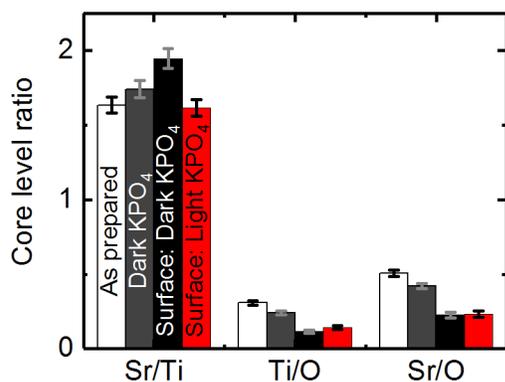

Figure S3: Narrowed region of surveys with an Al K-alpha source (IPE hv = 1486 eV) at 20° incidence to obtain more signal from the film surface. For the 4 nm $SrTiO_3$ after cycling in the dark (bold gray) and the 13 nm film after cycling in the dark (thin gray) and light (thin red), the lack of a peak in the highlighted region of the Pt 4f indicates no Pt is deposited during cycling.
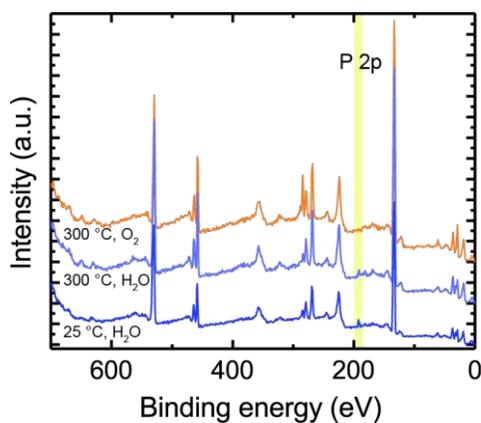
S2

Figure S4: Core level ratios probed with Al K-alpha source in UHV: Sr 3d, Ti 2p, Ge 3d, and O 1s for 4 nm $SrTiO_3$ / Ge. Error bars obtained from compounded standard deviations in CasaXPS. Compared to the 'as prepared' film measured directly after growth, the film HER cycled in 0.1 M potassium phosphate buffer (pH 7) maintains the same Sr/Ti ratio, giving no indication of preferential Sr leaching. However, the cycled film shows some reduction in the film peaks relative to the Ge substrate, indicating stoichiometric removal of the film during cycling – possibly due to corrosion of the underlying substrate at pinhole defects.
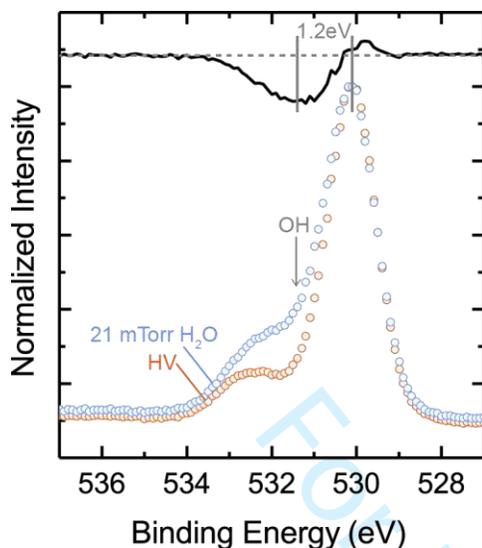

Figure S5: Chronoamperometry of bare Ge wafer at -0.77 V vs RHE in pH 7, 0.1 M phosphate buffer. The HER current decreases with time, and no change in current is observed with illumination by a 630 nm red LED.

Figure S6: Core level ratios probed with Al K-alpha source in UHV: Sr 3d, Ti 2p, and O 1s for 13 nm $SrTiO_3$ / Ge. Error bars obtained from compounded standard deviations in CasaXPS. Compared to the 'as prepared' film measured directly after growth measured at 90° (white), the film HER cycled in 0.1 M potassium phosphate buffer (pH 7) in the dark maintains the same Sr/Ti ratio when measured at 90° (dark gray), giving no indication of preferential Sr leaching. After cycling under illumination (20°, red), the Sr/Ti ratio at the surface decreases, potentially indicative of slight Sr leaching. The decrease in the Ti/O and Sr/O ratios decrease upon cycling is likely due to the formation of oxygen adsorbates from interaction with H_2O and/or the electrolyte.
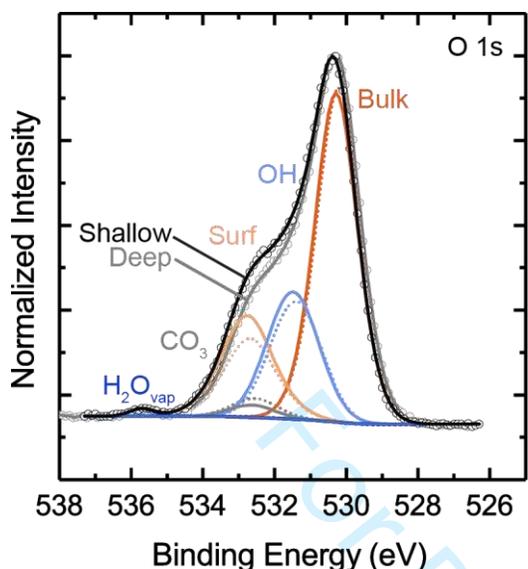

Figure S7: Surveys at an IPE of hv = 735 eV. The $SrTiO_3$ surface exhibits only the expected features from Sr, Ti, O and trace C at the noted temperature and 100 mTorr of the noted atmosphere, aside from a small intensity in the P 2p region likely attributed to PO_4 formation in H_2O.
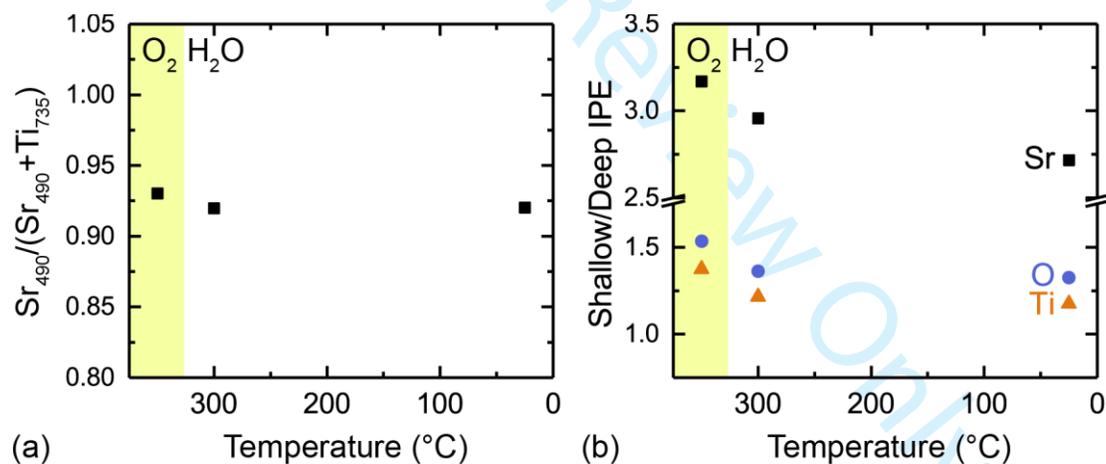
S4

Figure S8: O 1s spectra at 300 °C in high vacuum after O_2 exposure (orange) and while dosing H_2O, at ~21 mTorr H_2O (blue), probed with an IPE of $h\nu = 690$ eV. The difference spectra (black) illustrate that the OH species formed by H_2O dissociation on the surface are at ~1.2 eV above the bulk BE. The BE scale was calibrated using the Au 4f of a foil pressed onto the surface.

Table S1: O 1s fitting parameters in CasaXPS. GL indicates the percent Lorentzian component to a mixed Gaussian-Lorentzian line shape. The position of the surface feature was not constrained, but we note the fit for both O_2 and H_2O environments resulted in the component locating at ~532.7 eV. For OH and CO_3, the location was fixed relative to that of the bulk oxygen component. The BE scale was calibrated using the Au 4f of a foil pressed onto the surface.

	Bulk Ox	Surf	OH	CO$_3$	H$_2$O$_{vap}$
GL	40	50	0	0	0
FWHM	1-1.5	1.4-1.7	1.5-1.7	1.5-1.7	<1
Pos.		~532.7	+1.2	+2.35	

S5

Figure S9: Depth profiling of the O 1s core level at 300 °C in 100 mTorr H_2O, Shirley-background subtracted and normalized to the maximum intensity. Using a shallow incident photon energy (IPE, black/solid) of hv = 690 eV highlights species located on top of the bulk component (orange) – the "surface" peak (peach) and OH (light blue) – compared to the deep IPE (gray/dashed) of hv = 735 eV.

Figure S10: Quantification of surface stoichiometry during AP-XPS, measured at 300 °C in 100 mTorr O_2 (yellow bar) and at noted temperature in 100 mTorr H_2O (white region). (a) Cation ration: Sr 3d/(Sr 3d + Ti 2p), measured with an incident photon energy (IPE) of hv = 490 and 735 eV, respectively, to give comparable kinetic energies and thus inelastic mean free paths. (b) Ratio of shallow/deep IPE of Sr (black, 490 eV/690 eV), O (blue, 690 eV/735 eV), and Ti (orange, 690 eV/735 eV). All ratios remain similar regardless of sample temperature and environment, showing no indication of e.g. Sr segregation.